ChemComm

COMMUNICATION

A novel self-assembling nanoparticle of Ag–Bi with high reactive efficiency†

Jianyu Gong,[a] Chung-Seop Lee,[a] Yoon-Young Chang[b] and Yoon-Seok Chang*[a]

A novel Ag–Bi nanoparticle has been prepared *via* a facile precipitation approach. The nanoparticle could achieve purification of contaminated water without supplements and exhibited much higher activity compared to other popular nanoparticles (*e.g.* nZVI). The excellent performance of Ag–Bi was due in part to a large production of •OH radicals.

Environmental problems associated with harmful water pollutants pose severe threats to human health. "Green" water treatment methods are considered to be most optimal, and are therefore most often used. Over the past few decades, semiconductor photocatalysts, such as TiO_2, have received increasing attention because of their use in environmental pollution treatments under solar energy or visible light.[1] Often, the broad band gap of some photocatalysts limits the semiconductor use under solar light. As such, efforts have been made to address the inherent deficiency, using element doping, co-catalysts, morphology engineering, and others.[2] However, illumination requirements and complex semiconductor modifications limit the use of photocatalysts in real environments such as in river or in groundwater. Therefore, using other kinds of nanoparticles with zero valence is an attractive option. Among these, nano-sized zero valent iron (nZVI or Fe^0) is the one that has been widely used in environmental purification without supplements.[3] Unfortunately the low redox potential and weak reaction activity of nZVI limit its use in purifying most normal recalcitrant organic compounds (such as phenol) that could not be treated or mineralized by nZVI alone. Therefore, a novel nanoparticle design is badly needed to replace traditional photocatalysts or nZVI nanoparticles in pollution abatement.

Recently, a series of new catalysts based on silver, such as Ag_3PO_4, Ag_3AsO_4, and Ag_2O/Ag_2CO_3,[4–6] have shown significantly higher activity than the other currently known photocatalysts because of the effect of Ag^+ inside the catalyst lattice. On the other hand, an interesting element, bismuth (Bi), has been considered as a candidate for Bi-based catalyst fabrication due to its excellent electronic properties and a suitable conduction band.[7,8] For most Bi-based oxides (photocatalysts), the valence band (VB) is governed by O 2p and Bi 6s to narrow the band gap. Furthermore, the high catalytic activity of these materials is also ascribed to s composition in the VB because the photogenerated charge carriers in the s orbital have a high mobility, caused by the dispersive property of the Bi 6s orbital.[9]

In this study, we prepared a novel nanomaterial with zero chemical valence, Ag–Bi, through a facile precipitation process, easily treating phenol without any other supplement. Our study also investigated its crystalline structure, morphology, reactive activity, and degradation mechanism. To the best of our knowledge, this is the first report on Ag–Bi nanoparticles.

Fig. 1A presents a SEM image displaying the panoramic morphologies of the prepared particles. The image shows that the synthesized products are cotton-shaped with the main size distribution in the range of 150–220 nm (the inset of Fig. 1A) and have disordered mesoporosity between nanoparticles, confirmed by N_2 adsorption measurements (Fig. S1, ESI†). The nitrogen adsorption–desorption measurement results showed that the BET surface area of Ag–Bi was approximately 8 m^2 g^{-1}. This may be ascribed to the special porous structure of Bi, as shown in Fig. S2-A (ESI†), which significantly differs from the Ag structure (Fig. S2-B, ESI†). Fig. 1B shows the XRD pattern of the as-synthesized products. The diffraction peaks of Ag–Bi could be indexed to zero valent bismuth (JCPDS no. 010699) and zero valent silver (JCPDS no. 011167). No other peaks corresponding to bismuth oxides, silver oxides or other impurity phases were detected.

Fig. 1C shows the HRTEM image of the synthesized Ag–Bi, which is fully consistent with the SEM observations with respect to its morphology and dimensionality. The TEM images clearly demonstrate that the micro-net surface structure is an accumulation of many individual particles, with an average size

[a] *School of Environmental Science and Engineering, Pohang University of Science and Technology (POSTECH), Pohang, 790-784, Republic of Korea.*
  E-mail: yschang@postech.ac.kr; Fax: +82-54-279-8299; Tel: +82-54-279-2281
[b] *Department of Environmental Engineering, Kwangwoon University, Seoul, 139-701, Republic of Korea*

† Electronic supplementary information (ESI) available: Experimental details, materials characterization and Fig. S1–S8. See DOI: 10.1039/c4cc03300k
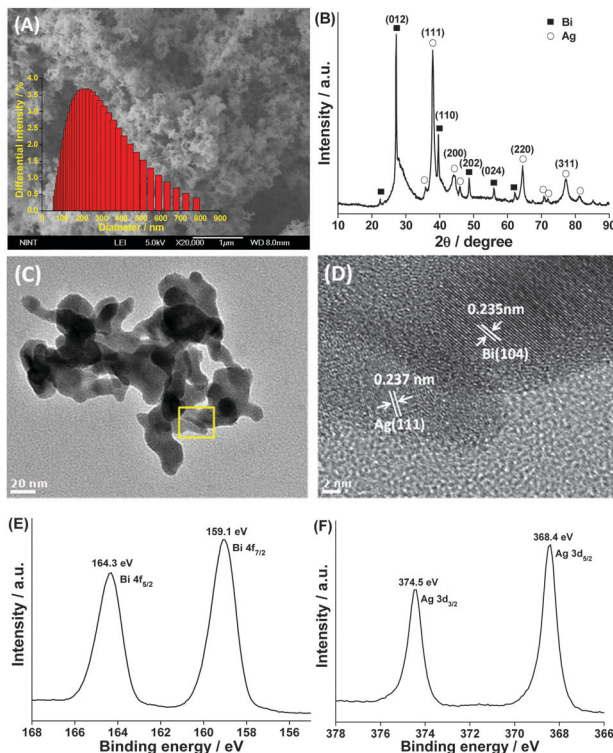
Fig. 1 (A) SEM image, (B) XRD pattern, (C) TEM image, (D) HRTEM image and XPS spectra of (E) the Bi 4f orbit and (F) the Ag 3d orbit of Ag–Bi nanoparticles. The inset of (A) shows the size distribution of Ag–Bi nanoparticles.

of 20 nm. These sheets intersect with each other, resulting in a net-like morphology with a porous structure. The porosity of the Ag–Bi nano-net was further confirmed by the clear lattice fringes shown in Fig. 1D and Fig. S3 (ESI†). The adjacent lattice planes correspond to the *d*-spacings of the Bi(104) and Ag(111) planes with values of 0.235 and 0.237 nm, respectively. The HRTEM images confirm that the synthesized Ag–Bi products have a highly crystalline structure, essential for high reactive activity. The elemental mapping analysis corresponding to the small area is shown in Fig. S4A and B (ESI†), confirming the coexistence of Ag and Bi, which are evenly distributed in the Ag–Bi composite (Fig. S4C and D, ESI†). Furthermore, the presence of Bi and Ag within the particles was also identified by the XPS global spectrum shown in Fig. S5 (ESI†). A trace amount of carbon in the spectrum was mainly attributed to the adventitious hydrocarbon from XPS itself.[10] Additionally, a small quantity of oxygen might be attributed to the exposure of Ag–Bi under room conditions.

Fig. 1E shows the high resolution XPS spectra of the Bi element. The peaks at 159.1 and 164.3 eV are associated with Bi $4f_{7/2}$ and Bi $4f_{5/2}$, respectively. The Ag 3d region (Fig. 1F) displays characteristic peaks at 368.4 and 374.5 eV, ascribed to the core levels of Ag $3d_{5/2}$ and Ag $3d_{3/2}$, respectively.

It is shown that the phenol degradation significantly depends on the mass ratio of Ag to Bi in Ag–Bi (Fig. 2A and Fig. S6, ESI†). An increase in the mass ratio from 0 to 0.5 correlates with an increase in phenol kinetic degradation (k_{obs}) from 0.114 h^{-1} to 0.978 h^{-1}. However, while the mass ratio of
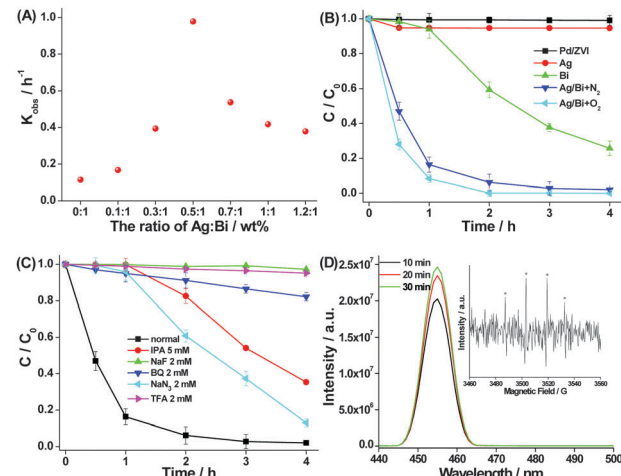

Fig. 2 (A) Plot of the phenol degradation rate constants *versus* the different mass ratios of Ag to Bi in Ag–Bi nanoparticles, (B) comparison of phenol degradation by different nanoparticles, (C) effects of different scavenger conditions on the oxidative degradation of phenol by Ag–Bi, (D) fluorescence spectra of umbelliferone in 0.1 mM coumarin solutions in the presence of Ag–Bi. The inset is the ESR spectral signal of DMPO–•OH spin-trapping in water in the presence of Ag–Bi after 2 min of reaction. (DMPO = 50 mM, Ag–Bi = 1 g L^{-1}).

Ag to Bi increases to 1.2, the k_{obs} of phenol decreases to 0.378 h^{-1}. This may be due to the dual roles of Ag. On the one hand, a higher Ag load will form a bimetallic structure with Bi, improving the reaction activity, because of fast electron transfer on the Ag surface. It will be discussed further below. On the other hand, since Ag cannot dispose of the organic pollutant on its own, an even higher Ag load decreases the relative amount of Bi in the bimetallic nanoparticles, resulting in the lower degradation (see Fig. 2B). As such, we selected the mass ratio of 0.5 (Ag : Bi) in Ag–Bi as the best option for further study.

Fig. 2B shows the phenol degradation timeframes when exposed to different nanoparticles. Ag–Bi demonstrated much higher degradation efficiencies than the others. After 2 h of treatment, almost 100% phenol was degraded by Ag–Bi. The phenol degradation rate with Ag–Bi was slightly improved in the presence of O$_2$. In the case of Bi alone, only 78% phenol was removed even after 4 h of treatment. On the other hand, there was only slight phenol degradation with nZVI (or Pd/ZVI),[11,12] widely used in pollution treatment.[3]

Next, we added a number of radical scavenging species to the combination of phenol with Ag–Bi, to determine the impact of intervention on degradation. These species included iso-propanol (IPA), sodium fluoride (NaF), 1,4-benzoquinone (BQ), sodium azide (NaN$_3$), and trifluoroacetic acid (TFA). The goal was to investigate contributory roles of any reactive •OH generated in the solution (•OH$_{bulk}$), •OH radicals on the surface of nanoparticles (•OH$_{ads}$), superoxide radicals (O$_2$•$^-$), singlet oxygen (^{1}O$_2$), and electrons (e$^-$).[13,14] Fig. 2C shows that, after 4 hours, the phenol concentration remains almost unchanged with the use of the •OH$_{ads}$ radical scavenger (NaF) and the electron radical scavenger (TFA). This suggests that the •OH$_{ads}$ and electrons are the dominant reactive species contributing to

the oxidative phenol degradation with Ag–Bi. In addition, due to the residual O_2 still remaining in the phenol liquid even after being purged with N_2, the phenol degradation efficiency decreased from 100% to 18% in the presence of the $O_2^{\bullet-}$ radical scavenger (BQ), implying that $O_2^{\bullet-}$ also plays a role with Ag–Bi. It might explain the better efficiency of phenol degradation at highly dissolved O_2 concentrations, as mentioned above (Fig. 2B). However, the phenol degradation efficiency decreased from 100% to 65% after 4 h in the presence of IPA, indicating that $^{\bullet}OH_{bulk}$ might be generated in small amounts in the system. When NaN_3 was added to the reaction, the degradation efficiency slightly decreased to 87% after 4 h, proving that $^1O_2$ was not critical in the whole reaction process. Therefore, the $^{\bullet}OH_{ads}$ radical should be the most important oxidizing species during the reaction.

To further assess $^{\bullet}OH_{ads}$ radicals produced during the reaction process, coumarin (0.1 mM) was used to monitor these radicals in the presence of Ag–Bi nanoparticles. Coumarin can react with $^{\bullet}OH$, forming highly fluorescent 7-hydroxycoumarin.[15] Fig. 2D shows that the increasing fluorescence intensities substantiate the production of $^{\bullet}OH_{ads}$ in the reactive process at the interface of Ag–Bi and water, which was also identified by the classical $1:2:2:1$ spectral signal of spin trapped DMPO–$^{\bullet}OH$, as shown in the inset of Fig. 2D. As far as we know, a portion of $^{\bullet}OH_{ads}$ is obtained by $O_2^{\bullet-}$ which tends to transform into $^{\bullet}OH$ in accordance with the following eqn (1) and (2):

$$e^- + O_2 \rightarrow O_2^{\bullet-} \tag{1}$$

$$2O_2^{\bullet-} + 2H_2O \rightarrow 2^{\bullet}OH + 2OH^- + O_2 \tag{2}$$
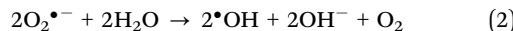
As such, the fluorescence spectra displayed might be due to the synthetic behavior of $O_2^{\bullet-}$ and $^{\bullet}OH_{ads}$, resulting in the excellent degradation of phenol with Ag–Bi. Furthermore, the concentration of $^{\bullet}OH_{ads}$ generated by Ag–Bi is almost two times higher than generated by nZVI (Fig. S7, ESI†), which is good evidence to illustrate that phenol can be treated by Ag–Bi more effectively than nZVI.

The high activity of Ag–Bi nanoparticles is assumed to be due to the metallic Ag^0 and Bi^0 species formed during the initial stage of the degradation process. Metallic Ag^0 serves as an excellent electron acceptor and efficiently traps the electrons. In addition, due to the local electromagnetic field and excellent conductivity of the Ag^0 species, electrons are generated from the transformation of Bi^0 to Bi^{3+} that can be quickly transferred to Ag^0.[16] The electrons trapped by the Ag^0 species further react with H_2O or O_2 molecules adsorbed on the composite surface to form active $^{\bullet}OH_{ads}$ radicals, or are directly involved in the degradation of phenol.

For investigation of the Ag–Bi phase transformation during this reaction, Fig. 3A shows the XRD patterns of Ag–Bi after sequenced phenol treatments. In process of time, Ag^0 converts into Ag_2O (JCPDS No. 120793). Turning to Bi^0, the XRD patterns also show the Bi_2O_3 (JCPDS No. 710467) transformation. The standard reduction potential of Ag^0/Ag^+ is +0.799 V and that of Bi^0/Bi^{3+} is +0.308 V; therefore, the electron transfer from Bi^0 to Ag^+ ions is thermodynamically favored, as shown by:

$$Bi^0 + 3Ag^+ \rightarrow 3Ag^0 + Bi^{3+} \tag{3}$$
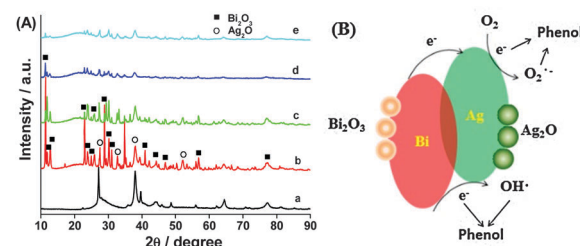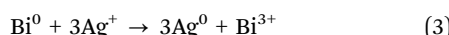
Fig. 3 (A) XRD patterns of (a) fresh Ag–Bi and Ag–Bi after (b) 1, (c) 2, (d) 3, and (e) 4 h sequential exposures in phenol solutions and (B) suggested mechanism for the degradation of phenol by Ag–Bi.

Most electrons generated from the transformation of Bi^0 to Bi^{3+} are transferred to the surface of Ag^0, resulting in the fast phenol degradation by Ag–Bi. In addition, as shown in Fig. S8 (ESI†), the morphology of Ag–Bi also changes after the degradation reaction. Compared to the fresh Ag–Bi (Fig. 1A), piece-like composites formed in the used Ag–Bi nanoparticles. The EDX analysis (the inset of Fig. S8, ESI†) shows that the piece-like composites (spectrum 1) are mainly formed by Bi atoms (9.93 at%), whereas the block-shaped particles (spectrum 2) are mainly formed by Ag atoms (20.55 at%). On the basis of these experimental results, the schematic in Fig. 3B outlines the basis for the significantly enhanced activity of Ag–Bi.

In this investigation, we successfully synthesized a novel highly reactive nanoparticle, Ag–Bi, through a facile precipitation approach. The newly developed Ag–Bi showed a zero valent chemical value. We then tested the reaction activity of Ag–Bi in phenol degradation, showing the complete removal efficiency resulting from its high concentration of $^{\bullet}OH_{ads}$ generated by Ag–Bi. This work presents an efficient nanoparticle that can be used to degrade persistent organic pollutants in wastewater without any other supplements. Furthermore, this new nanomaterial can also be applied to *ex situ* oxidation treatments of contaminated groundwater, while nZVI has been more efficiently used in *in situ* reductive remediation. The cost-effectiveness of this raw material was evaluated to compare with nZVI (ESI†). Although, considering the low toxicities of Ag[17] and Bi,[18] the biocompatibility is expected not to be a problem, its nanotoxicity and mobility should be tested prior to the field application.

Notes and references

1 N. Liu, X. Y. Chen, J. L. Zhang and J. W. Schwank, *Catal. Today*, 2014, **225**, 34.
2 S. Ardo and G. J. Meyer, *Chem. Soc. Rev.*, 2009, **38**, 115.
3 W. J. Liu, T. T. Qian and H. Jiang, *Chem. Eng. J.*, 2014, **236**, 448.
4 Z. G. Yi, J. H. Ye, N. Kikugawa, T. Kako, S. X. Ouyang, H. Stuart-Williams, H. Yang, J. Y. Cao, W. J. Luo, Z. S. Li, Y. Liu and R. L. Withers, *Nat. Mater.*, 2010, **9**, 559.
5 J. T. Tang, Y. H. Liu, H. Z. Li, Z. Tan and D. T. Li, *Chem. Commun.*, 2013, **49**, 5498.
6 C. L. Yu, G. Li, S. Kumar, K. Yang and R. C. Jin, *Adv. Mater.*, 2013, **26**, 892.
7 W. F. Su and Y. T. Lu, *Mater. Chem. Phys.*, 2003, **80**, 632.
8 S. L. Wang, W. H. Ma, Y. F. Fang, M. K. Jia and Y. P. Huang, *Appl. Catal., B*, 2014, **150–151**, 380.

9 J. W. Tang, Z. G. Zou and J. H. Ye, *J. Phys. Chem. C*, 2007, **111**, 12779.
10 J. G. Yu and X. X. Yu, *Environ. Sci. Technol.*, 2008, **42**, 4902.
11 B. P. Chaplin, M. Reinhard, W. F. Schneider, C. Schüth, J. R. Shapley, T. J. Strathmann and C. J. Werth, *Environ. Sci. Technol.*, 2012, **46**, 3655.
12 J. H. Kim, P. G. Tratnyek and Y. S. Chang, *Environ. Sci. Technol.*, 2008, **42**, 4106.
13 L. Zhou, W. Song, Z. Q. Chen and G. C. Yin, *Environ. Sci. Technol.*, 2013, **47**, 3833.
14 H. Hori, A. Yamamoto, K. Koike, S. Kutsuna, M. Murayama, A. Yoshimoto and R. Arakawa, *Appl. Catal., B*, 2008, **82**, 58.
15 K. Ishibashi, A. Fujishima, T. Watanable and K. Hashimoto, *Electrochem. Commun.*, 2000, **2**, 207.
16 D. W. Wang, Y. Li, G. L. Puma, C. Wang, P. F. Wang, W. L. Zhang and Q. Wang, *Chem. Commun.*, 2013, **49**, 10367.
17 S. Eckhardt, P. S. Brunetto, J. Gagnon, M. Priebe, B. Giese and K. M. Fromm, *Chem. Rev.*, 2013, **113**, 4708.
18 R. Mohan, *Nat. Chem.*, 2010, **2**, 336.